

# A Novel Isolated Current Sensor for High-Performance Power Electronics Applications

L. Dalessandro\*, N. Karrer<sup>†</sup>, J. W. Kolar\*

SWISS FEDERAL INSTITUTE OF TECHNOLOGY (ETH) ZURICH  
ETH-Zentrum, CH-8092 Zurich, Switzerland

\*Power Electronic Systems Laboratory  
E-mail: dalessandro@lem.ee.ethz.ch, kolar@lem.ee.ethz.ch  
<sup>†</sup>High Voltage Laboratory  
E-mail: nkarrer@eeh.ee.ethz.ch

**Abstract**—A planar current sensor, comprised of a magnetic current transformer and a Hall-effect element, is presented. The sensor has a broad frequency bandwidth from DC up to 30 MHz, a high current rating (40 A DC), superior linearity, high EMI immunity, small size, robustness and low realization cost. The main design formulations are given analytically; simulations and finite element results are presented for verification. Experimental results of current step response and  $dv/dt$  immunity are included.

## I. INTRODUCTION

Industrial electronic equipments for measurement [1], control [2], protection [3] and diagnostics [4] often require high-performance current sensors with features such as:

- 1) wide frequency bandwidth;
- 2) high current rating;
- 3) high  $dv/dt$  immunity;
- 4) linearity and stability with temperature variations;
- 5) compatibility with integration processes;
- 6) low realization effort and low cost.

The types of current sensors that have appeared in recent publications were based on numerous different physical effects, for instance magnetic coupling [5]–[7], magneto resistance [8], [9], Faraday induction [10], Hall effect [11] and zero flux [12]. However, as some recent comparative studies have shown [13]–[16], none of these sensors have really met all the requirements above listed in one device. A large bandwidth from DC [17] to several MHz has been the most difficult objective, but is also one of the most crucial characteristics for modern current controlled converters having switching frequencies up to 1 MHz and fast dynamics [18], [19]. Accuracy and low-cost of the sensing device are important requirements for current controlled converters. They are particularly crucial for direct pulsewidth modulation, such as hysteresis and direct power control, or for current sensor-based active ripple filters [20]. To circumvent these issues, many *sensorless* control techniques for converters and drives have been developed over recent years [21]. Another important aspect is the immunity of the sensor against external fields. For instance, a current sensor that is physically located near a SiC J-FET, can be affected severely by  $dv/dt$  transients up to several tens of  $kV/\mu s$  [22]. The parasitic coupling associated with the sensor itself can couple these transients into the sensing part causing distortion in the output. The sensor presented herein uses a planar current transformer (CT) as the main sensing device. For a high upper bandwidth limit the parasitic capacitance and leakage inductance must be small [23]. The number of turns on the sensing coil can therefore be reduced, which also decreases the value of the magnetizing inductance (cf.  $L_{m1}$  in

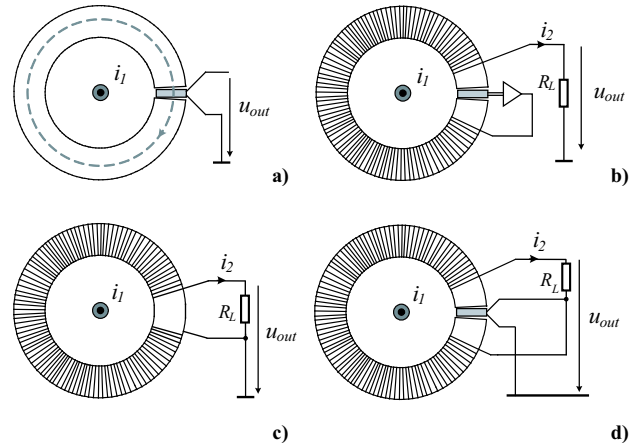


Fig. 1. Current sensors technologies based on magnetic core: (a) open-loop, (b) closed loop, (c) current transformer and (d) the proposed current sensor.

Fig. 5), thus providing some advantages [20]. The realization cost is lower for a planar transformer rather than a wire wound device. The drawback of this solution is that the lower corner frequency increases with fewer turns. This also happens when core materials with low permeability, a gapped or core-less transformers are used. Therefore, in order to extend the bandwidth to DC while keeping the advantages at high frequency, another device able to sense the DC and low frequency part of the measured signal can be combined with the CT. The technique of matching the frequency characteristics of two sensing devices for broad band current sensing from DC to several MHz has already been proposed in literature [5], [11], [24]–[26]. The proposed sensor features a Hall-effect based element for performing the low frequency current sensing. There are at least three well known architectures for combining a Hall-effect sensor and a magnetic core:

- 1) open loop;
- 2) closed loop;
- 3) a combination of open loop and CT.

For all three the Hall element is physically inserted into a gapped magnetic structure (cf. Fig. 1 a, b, d). A detailed description of each architecture is given in [13]. Closed loop devices are most common and operate on the principle of compensating the low frequency flux in the core with a feedback from a DC to low frequency sensor [25], [27], which is typically a Hall element. Since the magnetic core for a closed loop transducer operates at zero-flux, the operating point

of the sensor is also around the zero flux crossing. It is therefore unnecessary for the DC to low frequency sensor to be linear.

The proposed transducer uses a linear Hall element for sensing the current components from DC up to the lower corner frequency of the planar CT. The measured current signal is provided by the sum of the output signal of the Hall element and the CT (cf. Fig. 1d). Contrary to the closed loop technology, the proposed solution is passive and does not require feedback or process electronics. As described in detail in the following sections, the matching between the Hall element and the CT is provided without electronics stage, which is usually required for instance in [5]. The paper presents a planar prototype of the CT that is an improvement of a previous toroidal device [23]. It has been empirically verified that the main characteristics of DC-planar CT are:

- 1) frequency bandwidth from DC up to 30 MHz;
- 2) 40 A (DC) current rating;
- 3) high  $dv/dt$  immunity;
- 4) thermal stability (linear behavior under temperature variations);
- 5) compact planar transformer with a multilayer PCB winding;
- 6) low realization cost.

## II. MAGNETIC SYSTEM MODEL

The functioning of the sensor is dependent on two quantities: the magnetic flux  $\varphi$  within the core, that drives the Hall-effect element, and the output voltage  $u_L$  of the current transformer (cf. Fig. 3). The time dependence of  $\varphi$  and  $u_L$  can be analytically derived considering the equivalent model of the system depicted in Fig. 4. The model is based on the permeance-capacitance analogy. The magnetic and the electric circuits are coupled by Tellegen gyrators [23], [28]. This model presents numerous advantages: it allows implementation of frequency dependent components and complex permeability and allows access to the flux rate  $\xi$  and the magnetomotive force (MMF)  $\psi$ . Furthermore, since a resistance element in the permeance model represents magnetic losses (unlike the conventional magnetic reluctance model where resistance represents energy storage), core losses could be also extracted using this method.

In a previous work a HF permeance-model of the CT was presented [23]. Here, since the matching between the transfer functions (TF) of the two sensor components occurs in the kHz range, a low frequency model of the transformer is suitable for analyzing the proposed signal matching. Accordingly, skin and proximity effects in the windings, rotational magnetic losses and the secondary winding self capacitance are neglected.

The permeance model (cf. Fig. 2) is constructed defining the permeance,  $\Lambda$  in henries per turn square as

$$\Lambda = \frac{d\varphi}{d\psi} \quad (1)$$

where  $\varphi$  and  $\psi$  are the magnetic flux and MMF, respectively. The relation between charge  $q$  and voltage  $v$  across a capacitor is given

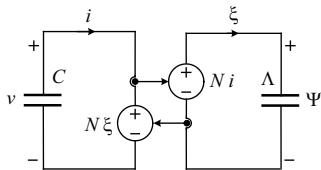


Fig. 2. Coupling between electrical and magnetic circuits using the permeance-capacitance analogy.

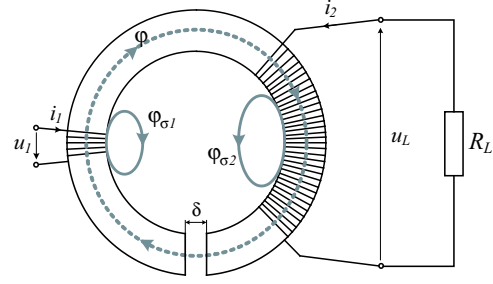


Fig. 3. Sketch of a current transformer.

by

$$\frac{dq}{dt} = C \frac{dv}{dt} \quad (2)$$

and can be written as

$$C = \frac{dq}{dv}. \quad (3)$$

From (1) and (3) it follows that the MMF  $\psi$  in ampere is used analogous to the voltage  $v$ , whereas the induced e.m.f. (electro motive force),

$$\xi = \frac{d\varphi}{dt} \quad (4)$$

is used analogous to the electrical current:

$$i = \frac{dq}{dt}. \quad (5)$$

The relation between the MMF  $\psi$  and the magnetic flux  $\varphi$  in a magnetic system can be therefore written in analogy to (2):

$$\frac{d\varphi}{dt} = \Lambda \frac{d\psi}{dt} \quad (6)$$

The magnetic and electric circuits are then coupled by a Tellegen gyrator,

$$\begin{aligned} v &= N\xi \\ \psi &= Ni \end{aligned} \quad (7)$$

where  $i$  and  $v$  are the current and voltage at the winding terminals,  $N$  the number of turns,  $\xi$  the induced voltage per turn and  $\psi$  the MMF.

Fig. 3 depicts a sketch of a current transformer comprised of  $N_1$  and  $N_2$  primary and secondary turns of resistance  $R_1$  and  $R_2$ , respectively, a load resistor  $R_L$ , and a gapped magnetic core, of air-gap  $\delta$ , cross sectional area  $A$  and flux pathlength  $l$  in the core.

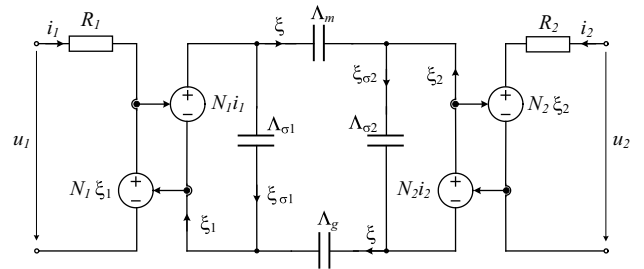


Fig. 4. Equivalent model of a transformer based on the permeance-capacitance analogy.

According to the transformer equivalent model shown in Fig. 4, the equations of the electric loops, considering (4) and (6), are:

$$\begin{aligned} u_1 &= R_1 i_1 + N_1 \frac{d\varphi_1}{dt} \\ u_2 &= R_2 i_2 + N_2 \frac{d\varphi_2}{dt} \end{aligned} \quad (8)$$

whereas the relations associated to the magnetic circuit are

$$\begin{aligned} \varphi_1 &= \varphi_{\sigma 1} + \varphi \\ \varphi_2 &= \varphi_{\sigma 2} - \varphi \end{aligned} \quad (9)$$

and

$$\begin{aligned} \varphi_{\sigma 1} &= \Lambda_{\sigma 1} N_1 i_1 \\ \varphi_{\sigma 2} &= \Lambda_{\sigma 2} N_2 i_2 \\ \varphi &= \left( \frac{\Lambda_m \Lambda_g}{\Lambda_m + \Lambda_g} \right) (N_1 i_1 - N_2 i_2). \end{aligned} \quad (10)$$

The primary and secondary leakage fluxes,  $\varphi_{\sigma 1}$  and  $\varphi_{\sigma 2}$ , are dependent on the permeances  $\Lambda_{\sigma 1}$  and  $\Lambda_{\sigma 2}$  of the leakage paths whereas the magnetizing flux  $\varphi$  is proportional to the resultant MMF and to the permeance of the air gap  $\Lambda_g$  which is much smaller than the core permeance  $\Lambda_m$ ,

$$\Lambda_g = \frac{\mu_0 A}{\delta} \ll \frac{\mu_0 \mu_r A}{l} = \Lambda_m \quad (11)$$

where  $\mu_0$  and  $\mu_r$  air and core permeability, respectively. By substituting (9) and (10) in (8) and considering (11), the primary voltage  $u_1$  is given by

$$\begin{aligned} u_1 &= R_1 i_1 + N_1 \frac{d\varphi_{\sigma 1}}{dt} + N_1 \frac{d\varphi}{dt} \\ &= R_1 i_1 + \Lambda_{\sigma 1} N_1^2 \frac{di_1}{dt} + \Lambda_g N_1^2 \frac{di_1}{dt} - \Lambda_g N_1 N_2 \frac{di_2}{dt} \end{aligned} \quad (12)$$

where

$$\begin{aligned} L_{\sigma 1} &= \Lambda_{\sigma 1} N_1^2 \\ L_{m1} &= \Lambda_g N_1^2 \\ M &= \Lambda_g N_1 N_2 \\ L_1 &= L_{\sigma 1} + L_{m1} \end{aligned} \quad (13)$$

are *leakage*, *magnetizing*, *mutual*, and *self*-inductances, respectively, of the primary winding.  $L_1$  and  $M$  can be measured,  $L_{m1}$  can be calculated and  $L_{\sigma 1}$  can be derived. These parameters can be determined by means of the well known open-circuit and short-circuit tests [29]. Equation (12) can be further arranged as follows

$$\begin{aligned} u_1 &= R_1 i_1 + L_{\sigma 1} \frac{di_1}{dt} + L_{m1} \frac{d}{dt} \left( i_1 - \frac{N_2}{N_1} i_2 \right) \\ &= R_1 i_1 + L_{\sigma 1} \frac{di_1}{dt} + L_{m1} \frac{di_{m1}}{dt} \end{aligned} \quad (14)$$

which corresponds to the primary side of the electrical circuit in Fig. 5. There, the currents  $i'_2$  and  $i_{m1}$  are defined respectively as:

$$i'_2 = \frac{N_2}{N_1} i_2 \quad (15)$$

$$i_{m1} = i_1 - i'_2 \quad (16)$$

In a similar fashion, the output voltage  $u_2$  can be written from (8) and (9) as

$$u_2 = R_2 i_2 + N_2 \frac{d\varphi_{\sigma 2}}{dt} - N_2 \frac{d\varphi}{dt} \quad (17)$$

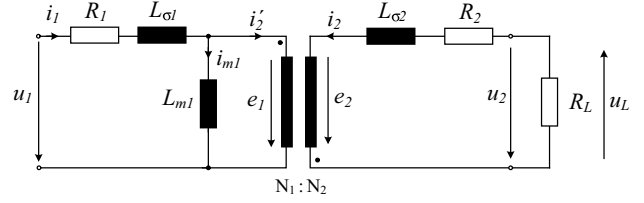


Fig. 5. Equivalent electric circuit of a current transformer.

and, analogous to (13), the *leakage*, *magnetizing*, *mutual*, and *self*-inductances of the secondary winding can be defined as follows:

$$\begin{aligned} L_{\sigma 2} &= \Lambda_{\sigma 2} N_2^2 \\ L_{m2} &= \Lambda_g N_2^2 \\ M &= \Lambda_g N_2 N_1 \\ L_2 &= L_{\sigma 2} + L_{m2}. \end{aligned} \quad (18)$$

The e.m.f.  $e_2$  induced in the secondary by the mutual flux  $\varphi$ , is defined as

$$e_2 = N_2 \frac{d\varphi}{dt} \quad (19)$$

and it drives the secondary current  $i_2$ . The e.m.f.  $e_1$  induced across the primary winding is similarly given by

$$\begin{aligned} e_1 &= N_1 \frac{d\varphi}{dt} \\ &= L_{m1} \frac{di_{m1}}{dt} \end{aligned} \quad (20)$$

and it is related to  $e_2$  through the transformer ratio:

$$\frac{e_2}{e_1} = \frac{N_2}{N_1}. \quad (21)$$

This latter and (15) constitute the equations of an ideal transformer, *i.e.* core permeability  $\mu_r$  infinite and magnetic flux  $\varphi$  zero. The (17) can be written as

$$e_2 = R_2 i_2 + L_{\sigma 2} \frac{di_2}{dt} - u_2 \quad (22)$$

Let define  $R_L$  and  $u_L$  as the load resistor and load voltage:

$$\begin{aligned} u_L &= R_L i_2 \\ &= -u_2. \end{aligned} \quad (23)$$

Considering (16), (20), (21) and (23), it follows

$$\begin{aligned} \frac{N_2}{N_1} \left( L_{m1} \frac{d}{dt} \left( i_1 - \frac{N_2}{N_1} i_2 \right) \right) &= R_2 i_2 + L_{\sigma 2} \frac{di_2}{dt} + u_L \\ M \frac{di_1}{dt} - L_{m2} \frac{di_2}{dt} &= R_2 i_2 + L_{\sigma 2} \frac{di_2}{dt} + R_L i_2 \\ M \frac{di_1}{dt} &= R_2 i_2 + L_2 \frac{di_2}{dt} + R_L i_2 \end{aligned} \quad (24)$$

Using the Laplace transform, where  $s$  indicates the Laplace operator, from (24) the ratio between primary and secondary currents is then provided by:

$$\begin{aligned} \frac{I_2}{I_1} &= \frac{sM}{R_2 + R_L + sL_2} \\ &= \frac{N_1}{N_2} \frac{sL_{m2}}{R_2 + R_L + sL_2} \\ &= \frac{N_1}{N_2} \frac{s \frac{L_{m2}}{R_2 + R_L}}{1 + s \frac{L_2}{R_2 + R_L}}. \end{aligned} \quad (25)$$

### III. PRINCIPLE OF OPERATION

#### A. Ideal Sensor

If the leakage inductance  $L_{\sigma 2}$  is sufficiently small, which is typical for planar transformer, then

$$L_2 \approx L_{m2} \quad (26)$$

and, if the winding resistance  $R_2$  is negligible with respect to the load resistor  $R_L$ , then the time constant associated with the secondary winding assumes the form:

$$\tau = \frac{L_2}{R_L}. \quad (27)$$

Accordingly, the current ratio (25) can be written as

$$\frac{I_2}{I_1} = \frac{N_1}{N_2} \frac{s\tau}{1+s\tau}. \quad (28)$$

The expression of the flux  $\varphi$  in the frequency domain is obtained from (10), (11) and (28):

$$\begin{aligned} \Phi &= \Lambda_g(N_1 I_1 - N_2 I_2) \\ &= N_1 \Lambda_g \left(1 - \frac{N_2}{N_1} \frac{I_2}{I_1}\right) I_1 \\ &= N_1 \Lambda_g \left(\frac{1}{1+s\tau}\right) I_1. \end{aligned} \quad (29)$$

The Hall-effect element measures the DC to low frequency components of the current  $i_1$ . It uses the magnetic flux density  $B$ , defined as

$$B = \frac{\Phi}{A} \quad (30)$$

generated by the current  $i_1$ , to deflect an *internal* current flowing through a conductor, thus developing a transversal potential. The output voltage signal of the Hall-effect element  $U_H$  is proportional to  $B$  through the sensitivity  $S_{Hall}$ , measured in V/T, and is given by

$$U_H = S_{Hall} B. \quad (31)$$

The TF of the Hall captor  $U_H/I_1$  can finally be derived by substituting (11), (29) and (30) in (31) and assuming  $N_1=1$ :

$$\begin{aligned} \frac{U_H}{I_1} &= \frac{\mu_0}{\delta} S_{Hall} \left(\frac{1}{1+s\tau}\right) \\ &= k_H \left(\frac{1}{1+s\tau}\right). \end{aligned} \quad (32)$$

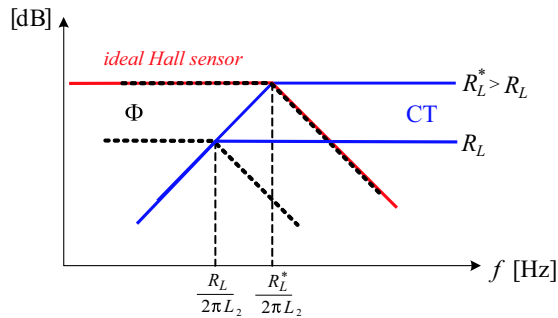


Fig. 6. Resulting transfer function of the proposed transducer. The matching between the two sensors is achieved by using an opportune value of the transformer's load resistor  $R_L$  (36).

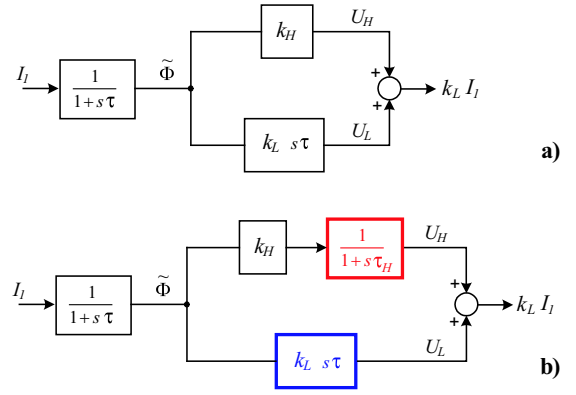


Fig. 7. Block diagrams explaining the functioning of the proposed current sensor when  $k_H = k_L$ : a) ideal and b) real operating.

On the other side, the TF of the current transformer  $U_L/I_1$  is derived by (23) and (25):

$$\begin{aligned} \frac{U_L}{I_1} &= \frac{R_L}{N_2} \frac{s\tau}{1+s\tau} \\ &= k_L \frac{s\tau}{1+s\tau}. \end{aligned} \quad (33)$$

Let observe that (32) is a low pass function and the (33) a high pass function having the same corner frequency as depicted in Fig. 6.

In the proposed current sensor the output signal is provided by

$$U_{out} = U_L + U_H \quad (34)$$

and these voltages are summed without using process electronics (cf. Fig. 1d). If the gain values of the sensor components are designed to be equal, then the overall transfer function of the sensor, provided by

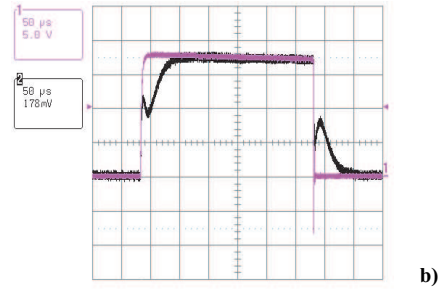
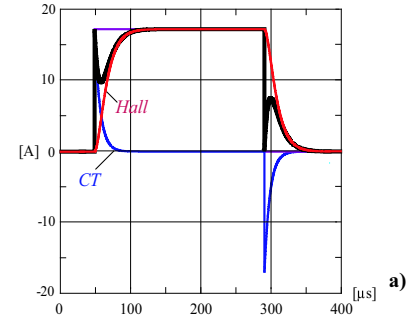


Fig. 8. Sensor components that contribute to the formation of the current step; operating principle according to Fig. 7b. The sum between the Hall captor and the CT output signals does not reproduce properly the step because  $\tau_H \approx \tau$ : a) simulation and b) measurement.

the sum of (32) and (33) is a flat response over the entire frequency band (cf. Fig. 6). Constraining the gain of each of the two transfer functions to be equal in value yields

$$\frac{R_L}{N_2} \equiv \frac{\mu_0}{\delta} S_{Hall} \quad (35)$$

If the parameters  $N_2$ ,  $S_{Hall}$  and  $\delta$  have already been selected, then the value of the load resistance  $R_L$  has to be chosen such that:

$$R_L = \frac{N_2 \mu_0 S_{Hall}}{\delta} \quad [\Omega] \quad (36)$$

In Fig. 7a the block diagram that explains the functioning of the sensor is shown. There, a quantity proportional to the flux  $\Phi$  drives both the Hall-effect element and the current transformer, whose output signals,  $U_H$  and  $U_L$ , are summed to provide in output a constant gain equal to

$$U_{out} = k_L I_1. \quad (37)$$

### B. Real Sensor

The ideal functioning of the sensor has been derived under the assumption of constant sensitivity of the Hall captor (31). Actually, the Hall sensor is better characterized by a low pass function as:

$$U_H = \frac{S_{Hall}}{1 + s\tau_H} B. \quad (38)$$

where  $\tau_H$  is the time constant of the device. The block diagram that describes the real functioning of the sensor is depicted in Fig. 7b. If the Hall element corner frequency  $f_H$ ,

$$f_H = \frac{1}{2\pi\tau_H} \quad (39)$$

is at least one decade larger than the CT's lower corner frequency  $f$  given by

$$f = \frac{1}{2\pi\tau} = \frac{R_L}{2\pi} \frac{\delta}{\mu_0 N_2^2 A} \quad (40)$$

such that the condition

$$f_H \gg f \quad (41)$$

is verified, then matching between the output signals of Hall element and CT occurs correctly. Equation (41) ensures that the Hall-element operates in the linear part of its characteristic curve and that no further attenuation occurs by the matching point.

In case

$$\tau_H \approx \tau \quad (42)$$

then the Hall captor output signal is affected by delay, as shown in the simulation in Fig. 8a and in the measurement Fig. 8b, and the sum between the signal components of Hall and CT does not reproduce properly the current step. Therefore, the values of  $R_L$  and  $L_2$  must be selected carefully to obtain a corner frequency  $f$  sufficiently smaller than  $f_H$ .

Moreover, the parameters  $L_{\sigma 2}$  and  $R_2$  affect the real operating of the sensor and it is opportune to include them in design and model. Although a planar transformer shows a smaller leakage inductance than a toroidal device, the  $L_{\sigma 2}$  plays an increasing role at high frequency and it determines with the winding self capacitance  $C$  the upper bandwidth limit of the transformer. The value of winding resistance  $R_2$  is dependent on the cross-section of the secondary turns; although a compact secondary coil is desirable to obtain a small device, a larger wire cross section ensures a lower winding resistance, hence a lower corner frequency  $f$ , (25).

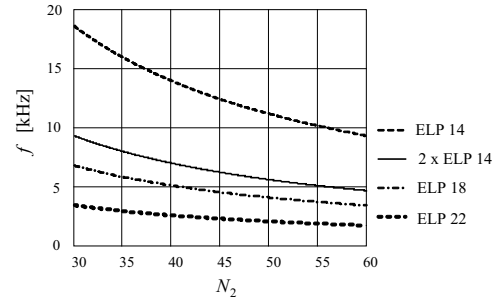


Fig. 9. Dependency of the planar CTs' lower corner frequency  $f$  on the number  $N_2$  of secondary turns for different ELP cores.

## IV. REALIZATION OF THE PROTOTYPE

A toroidal prototype of the proposed current sensor was shown in [23]. The device was made out of a toroidal gapped magnetic core and a Hall element positioned in the air gap. An electric screen between the primary was used to split the interwinding capacitance and to decrease the value of the leakage inductance [30]. The choice of the planar shape rather than the toroidal one leads to a significative improvement of the frequency behavior of the device and brings with it the following advantages while still retaining all the features of the toroidal prototype:

- 1) higher frequency bandwidth;
- 2) a low profile;
- 3) an embedded primary conductor in the component, and better control over parasitics;
- 4) better manufacturability;
- 5) the ability to integrate all the main parts, i.e. windings, EM screens, process electronics into a compact and mechanically robust device.

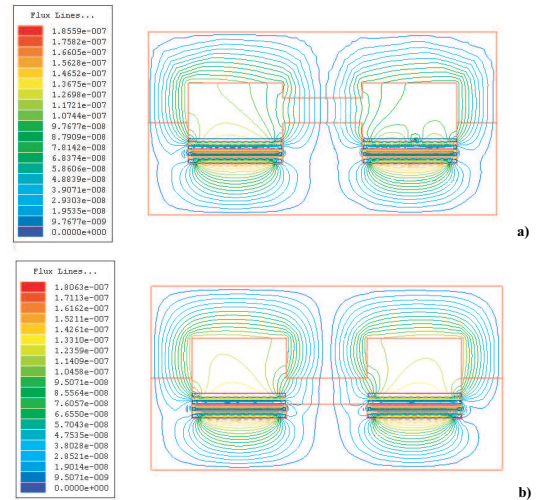


Fig. 10. Magnetic flux lines distribution within the core for a frequency of 1 kHz. This frequency corresponds to the end of the operating region of the Hall element and the beginning of the transformer's. It is important that the flux lines link the Hall element and remain within the air gap. Therefore the solution (a) of having the air gap far from the winding-PCB layer is more convenient than having the air gap aligned with the winding PCB (b).

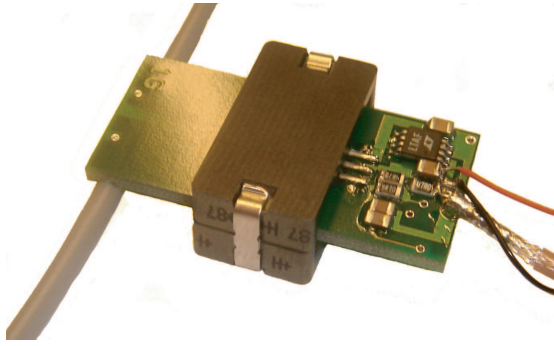


Fig. 11. Photograph of the proposed DC planar-CT featuring a planar ELP18 core.

With these aims in mind, a planar magnetic core in combination with an eight-layers PCB was built: four layers host the secondary coil of 45 turns, one layer for the primary, one for the output stage electronics, and the remaining two layers for ground plane and screen. The core consists of two E-cores with an air gap of 1.4 mm. In order to design a sufficiently compact planar prototype, the smallest commercial ELP ferrite cores were selected [31]. They are ELP14,

ELP18 and ELP22. To reduce the parasitics associated with the windings and to decrease the number of layers of the PCB, the number of secondary turns was selected to be the minimum possible for proper sensor operation.

For this aim, the value of the the corner frequency  $f$  has been calculated as a function of the number  $N_2$  of secondary turns for four different planar cores. The results of the calculations are shown in the curves of Fig. 9. Since a sufficient large value of the inductance  $L_2$  is desired in order to fulfill (41), the solution of taking two ELP14 cores has also been considered. An Allegro A3515 Hall element [32] was chosen for its linear characteristic up to 30 kHz. Therefore only two cores, ELP18 and ELP22, with a number of turns larger than 40 fulfill (41) and present lower corner frequencies below 5 kHz. Moreover, it is important that the flux lines link the Hall element and remain within the cross-section of the air gap until the CT start working within the linear part of its frequency characteristic: this has been verified by FEM simulations shown in Fig. 10.

On the basis of these considerations, 18 different prototypes were built, with different combinations of winding strategies and layers arrangements. A photograph of the proposed DC planar-CT that features a ELP18 planar core is shown in Fig. 11.

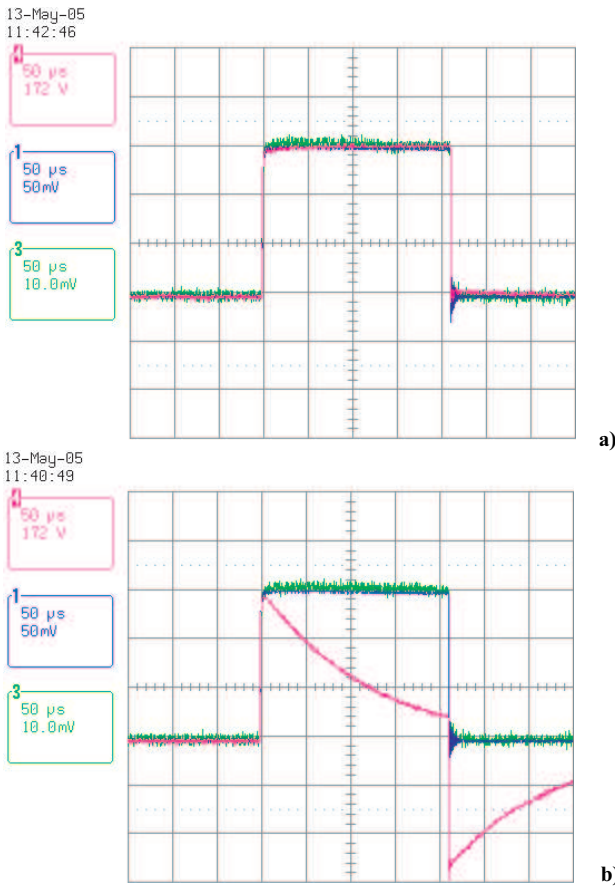


Fig. 12. (a) Current step response where the sensors are respectively: Ch. 1 Shunt LEM 25/10, Ch. 3 Tektronix A6312 Probe, Ch. 4 proposed DC planar-CT current sensor. Vertical scale 5 A/div, time scale 50  $\mu$  s/div. In (b) the Hall sensor signal is not present; only the planar current transformer is sensing.

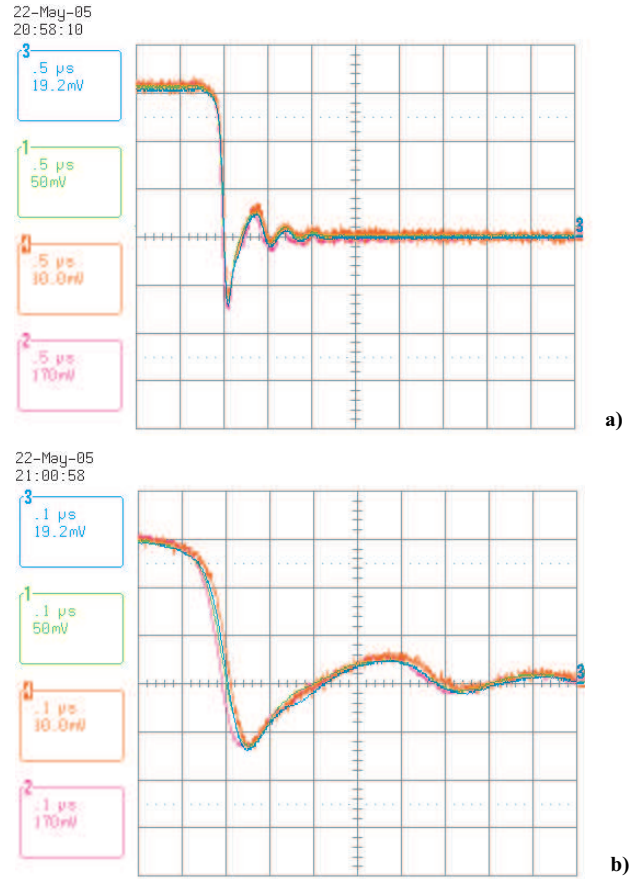


Fig. 13. Current step response where the sensors are respectively: Ch. 1 Shunt LEM 25/10, Ch. 2 proposed DC planar-CT current sensor, Ch. 3 HOKA sensor [5], Ch. 4 Tektronix A6312. Vertical scale 5 A/div, time scale: (a) 0.5  $\mu$  s/div, (b) 0.1  $\mu$  s/div. Furthermore (b) shows 20 ns delay of the Tek probe.

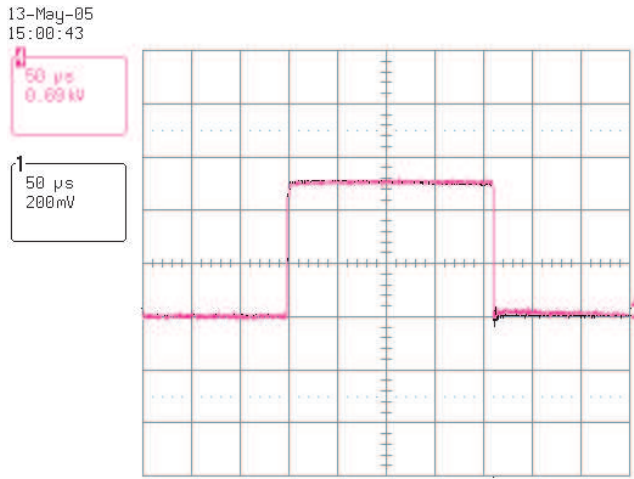


Fig. 14. Current step response where the sensors are respectively: Ch. 1 Shunt LEM 25/10, Ch. 4 proposed DC planar-CT current sensor. Vertical scale 20 A/div, time scale: 50  $\mu$ s/div.

## V. EXPERIMENTAL RESULTS

### A. Current Step Response

A rectangular shaped current waveform contains more harmonic components than other waveforms, for instance a triangular one, and is therefore a very effective test for a current sensor. The current step response of the proposed DC-planar CT was compared with three other wide-bandwidth devices: a Tektronix A6312 probe (100 MHz), a Shunt LEM 25/10 (10 MHz) and a HOKA Probe (50 MHz) [5]. The measurement results are shown in Figs. 12-14, and the performance of the proposed sensor compares equally well to the other more expensive and well established current transducers. The high upper bandwidth limit of the CT, measured 30 MHz according to the procedure presented in [23], allows faithful reproduction of the rising and falling edges of the current step (cf. Figs. 12-13) while the Hall-element detects the stationary edges of the signal.

### B. Core Saturation

A closed loop implementation of the sensor ensures that the magnetic core saturates at higher rating of primary current than an open loop architecture. For a closed loop sensor, the magnetic field in the core is compensated by the feedback action of the DC to low frequency sensor whose output signal is injected in the secondary winding to oppose the primary MMF (cf. Fig. 1b). If the primary current  $i_1$  is stationary (DC), there is no flux rate, hence the CT is inhibited and does not provide any output signal.

An issue for the proposed sensor is the saturation of the magnetic core, since no compensation loop is implemented. However, the quite large air-gap, necessitated by the physical dimensions of the Hall element, reduces the effects of the non linear magnetic characteristic of the core and stabilizes the value of the inductance  $L_{m1}$ . This latter becomes less dependent from the core parameters, (11), and decreases in value, because the equivalent permeability of the gapped system is smaller than the core permeability.

Since the volt-seconds necessary to saturate a magnetic circuit (starting from  $B = 0$ ) are

$$\begin{aligned} \varphi_S &= N_1 B_S S \\ &= L_{m1} i_S, \end{aligned} \quad (43)$$

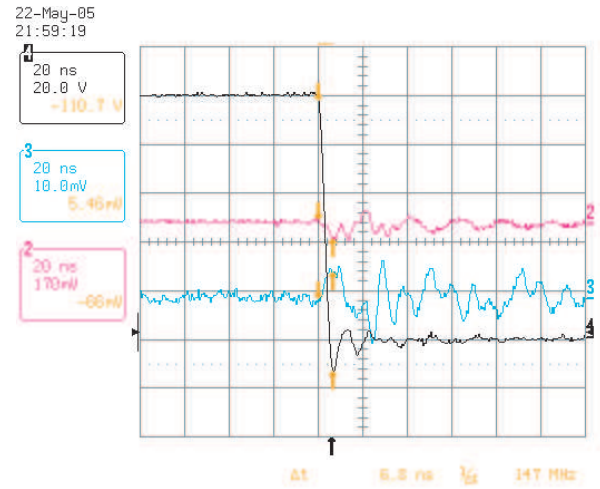


Fig. 15.  $dv/dt$  immunity test. Ch. 2 proposed DC planar-CT current sensor, Ch. 3 Tektronix A6312, Ch. 4 voltage step (16 kV/ $\mu$ s). Time scale: 20 ns/div; voltage scale: 20 V/div; current scale 0.5 A/div.

increasing the air-gap length reduces the inductance value according to (10) and (11), whereas the current  $i_S$ , for which saturation occurs, increases.  $\varphi_S$  and  $B_S$  indicate saturation flux and induction, respectively. Fig. 14 shows a 0.2 ms current step of 50 A in amplitude; the sensor is able to measure such current steps. By means of similar tests, an excellent linear behavior has been registered up to 40 A DC.

### C. $dv/dt$ Immunity Test

Whenever there is a high  $dv/dt$ , the interwinding capacitance of the CT couples the primary and secondary windings and transfers to the secondary the disturbance in form of CM current. In particular, if the setup is such that the current sensor is placed near a power MOSFET, the device is then stressed with severe  $dv/dt$ , where  $v$  is namely the drain to source voltage. One measurement result of  $dv/dt$  immunity is shown in Fig. 15. The measurement setup adopted to produce the voltage step was similar to the one used to generate the current step. However, a faster switch (FET) was inserted in the measurement circuit that presented a very large load resistor (3 k $\Omega$ ), hence the current flowing was nearly zero. In this way, the current measured by the sensors under test was due just to the parasitic capacitances that couple the transients  $dv/dt$  into the output of the sensor. The distortion registered in output of the proposed sensor for 16 kV/ $\mu$ s voltage rate is comparable to the performance of a Tektronix A6312 used as reference device (cf Fig. 15).

## VI. CONCLUSION

This paper has presented a novel isolated current sensor made out of the combination of a Hall-effect element, positioned in the air gap of the magnetic structure, and a planar current transformer with a multilayer PCB winding. The Hall captor is sensitive to the DC to low frequency components of the measured current, whereas the higher frequencies, to which the Hall sensor is insensitive, are detected magnetically by the CT. The matching between the Hall element and the CT is performed without electronic stage. The functioning has been explained analytically by means of a permeance model of the transformer. This model allows access to the flux, flux rate and MMF besides the electrical quantities. Furthermore it allows time and frequency simulations on electrical network simulators of electro-magnetic networks; it allows implementation of

frequency dependent components, complex permeability and direct core losses extraction.

Simulations and FEM results have been presented for verification. It has been shown that the appropriate dimensioning of the magnetic system, and especially the accurate selection of the corner frequency  $f$  of the CT transfer function is important to grant the correct functioning of the sensor.

The choice of the planar magnetic structure led to the following advantages, while still retaining all the features of a former toroidal prototype [23]: higher frequency bandwidth, low profile, better manufacturability and compatibility with integration processes.

Furthermore, a planar prototype has been shown and the following features have been verified experimentally: frequency bandwidth from DC up to 30 MHz, high current rating (40 A DC), superior linearity, high immunity against  $dv/dt$  transients.

All these performances, in particular accuracy and low realization cost, comply with the requirements necessary for the application of the sensor within the latest generation of converters and drives.

## VII. ACKNOWLEDGEMENTS

The authors would like to thank P. Furrer and P. Seitz for their assistance in constructing the prototypes.

## REFERENCES

- [1] F. Costa, P. Poulichet, F. Mazaleyrat, and E. Labouré, "The current sensors in power electronics, a review," *EPE Journal*, vol. 11, pp. 7–18, Oct 2001.
- [2] D. Y. Qiu, S. C. Yip, H. Shu-Hung Chung, and S. Y. Ron Hui, "On the use of current sensors for the control of power converters," *IEEE Tran. Power Electronics*, vol. 18, pp. 1047–1052, July 2003.
- [3] L. A. Kojovic, "Guidelines for current transformers selection for protection systems," *Proceedings of Power Engineering Society Summer Meeting*, pp. 593–598, 2001.
- [4] J. R. Stack, T. G. Habetler, and R. G. Harley, "Bearing fault detection via autoregressive stator current modeling," *IEEE Tran. Industry Application*, vol. 40, pp. 740–747, May-June 2004.
- [5] N. Karrer and P. Hofer-Noser, "A new current measuring principle for power electronics applications," *Proceedings of Information Storage and Processing Conference*, pp. 279–282, 1999.
- [6] C. Oates, A. J. Brunett, and C. James, "The design of high performance Rogowski coils," *Proceedings of Power Electronics, Machines and Drives Conference*, pp. 568–573, 2002.
- [7] L. Zhao, J. D. van Wyk, and W. G. Odeendal, "Planar embedded pick-up coil sensor for integrated power electronics modules," *Proceedings of Applied Power Electronics Conference*, pp. 945–951, 2004.
- [8] G. Laimer and J. W. Kolar, "Design and experimental analysis of a DC to 1 MHz close loop magnetoresistive current sensor," *Proceedings of Applied Power Electronics Conference*, pp. 1288–1292, 2005.
- [9] L. Di Rienzo, R. Bazzocchi, and A. Manara, "Circular arrays of magnetic sensors for current measurements," *IEEE Tran. Instrumentation Measurements*, vol. 50, pp. 1093–1096, Oct. 2001.
- [10] FOCS, "Fiber optic current sensors," *Available Online: www.abb.com*, 2005.
- [11] L. Ghislanzoni and J. A. Carrasco, "A DC current transformer for large bandwidth and high common mode rejection," *IEEE Tran. Industrial Electronics*, vol. 46, pp. 631–636, June 1999.
- [12] LEM, "Current sensors," *Available Online: www.lem.com*, 2005.
- [13] E. Favre and W. Teppan, "State of the art in current sensing technologies," *Proceedings of Power Electronics and Intelligent Motion Conference*, pp. 549–554, Nov. 2003.
- [14] C. Xiao, L. Zhao, T. Asada, W. G. Odeendal, and J. D. van Wyk, "An overview of integrable current sensors technologies," *Proceedings of Power Electronics Specialist Conference*, pp. 1252–1257, 2003.
- [15] P. Ripka, "Current sensors using magnetic materials," *International Journal of Optoelectronics and Advanced Materials*, vol. 6, pp. 587–592, June 2004.
- [16] F. Costa, E. Labouré, F. Forest, and C. Gautier, "Wide bandwidth, large AC current probe for power electronics and EMI measurements," *IEEE Tran. Industrial Electronics*, vol. 44, pp. 502–511, Aug. 1997.
- [17] H. G. Sauer, "Influence of the dc current on the operating of a current transformer," *Messen+Prüfen/Automatik (in German)*, pp. 267–275, June 1975.
- [18] G. Laimer and J. W. Kolar, "Wide bandwidth low complexity isolated current sensor to be employed in a 10kW/500kHz three-phase unity power factor PWM rectifier system," *Proceedings of Power Electronics Specialist Conference*, pp. 1065–1070, 2002.
- [19] J. Pankau, D. Leggate, D. Schlegel, R. Kerkman, and G. Skibiniski, "High frequency modelling of current sensors," *IEEE Tran. Industrial Applications*, vol. 35, pp. 1374–1382, Nov.-Dec. 1999.
- [20] M. Zhu, D. J. Perreault, V. Caliskan, T. C. Neugebauer, S. Guttowski, and J. G. Kassakian, "Design and evaluation of feedforward active ripple filters," *IEEE Tran. Power Electronics*, vol. 20, pp. 276–285, March 2005.
- [21] M. P. Kazmierkowski, R. Krishnan, and F. Blabjeerg, *Control in Power Electronics*. Academy Press, 2002.
- [22] S. Round, M. Heldwein, J. W. Kolar, A. Melkonyan, and I. Hofsjager, "A SiC JFET driver for a 5 kW, 150 kHz three-phase PWM converter," *Proceedings of Industrial Applications Society Conference*, pp. 410–416, 2005.
- [23] L. Dalessandro, W. G. Odeendal, and J. W. Kolar, "HF characterization and non-linear modeling of a gapped toroidal magnetic structure," *Proceedings of Power Electronics Specialist Conference*, pp. 1250–57, 2005.
- [24] L. Ghislanzoni, "Magnetic coupled current sensing techniques for spacecraft systems," *Proceedings of European Space Power Conference*, pp. 323–327, 1989.
- [25] K. Unser, "Beam current transformers with DC to 200 MHz range," *IEEE Tran. Nuclear Science*, pp. 934–938, June. 1969.
- [26] J. Weber, *Oscilloscope probe circuits*. Tektronix Inc., 1969.
- [27] S. Ogasawara, K. Murata, and H. Akagi, "A digital current sensor for PWM inverters," *Proceedings of the Industrial Application Society Conference*, pp. 949–955, 1992.
- [28] R. W. Buntentbach, "Analogues between magnetic and electrical circuits," *Electronics Products*, pp. 108–113, Oct. 1969.
- [29] A. E. Fitzgerald, C. Kingsley, and S. D. Umans, *Electric Machinery*. McGraw Hill, 2003.
- [30] E. Labouré, F. Costa, and F. Forest, "Current measurement in static converters and realization of a high frequency passive current probe," *Proceedings of European Power Electronics Conference*, pp. 478–483, 1993.
- [31] EPCOS Ferrites, "Datasheets and specifications," *Available Online: www.epcos.com*, 2005.
- [32] Allegro, MycroSystems, Inc., "Linear Hall Sensors.," *Available Online: www.allegromicro.com*, 2005.